SIMULATION OF A GAS JET ENTERING A FAILED STEAM GENERATOR DURING A SGTR SEQUENCE: VALIDATION OF A FLUENT 6.2 MODEL

C. López del Prá, F. J. S. Velasco, L. E. Herranz

Unit of Nuclear Safety Research, CIEMAT, Madrid (SPAIN)

Abstract

This paper summarizes the major insights of gas jets entering a tube bundle from either a guillotine or a fish-mouth breach. This scenario is highly relevant in nuclear safety since it determines the potential retention of radioactive particles during risk-dominant sequences, the so called Steam Generator Tube Rupture (SGTR) sequences. The scenario has been modeled with the FLUENT 6.2 code and its predictions have been proven to be grid independent and consistent with the experimental data available. The topology of the jets and the influence of the inlet mass flow rate (from 75 to 250 kg/h) have been studied in terms of velocity profiles.

The results show that the breach shape heavily determines the jet topology. Both jets initially describe a quasi-parabolic trajectory, which is affected by the presence of the tubes. A guillotine breach generates a jet with azimuthal symmetry, which vanishes for the fish-mouth breach configuration. In this case, jet expands azimuthally in a pseudo-triangular way with a small angle. This fact diminishes the momentum loss across the bundle, so that for the same inlet mass flow rate the fish-mouth jet penetration is higher than the guillotine one. The normalized maximum radial and axial velocities of the jet from the guillotine breach are found to be self-similar with respect to inlet mass flow rate along the tube row position and axial distance to the breach, respectively. However, in absolute terms higher penetrations are found at higher mass flow rates.

Nomenclature

CAHT	Ciemat Artist hydrodynamics tests
C_D	Drag coefficient
D,d	tube diameter
D_h	hydraulic diameter
h	breach height
h_s	specific enthalpy
K	turbulent kinetic energy
k_l	pressure loss coefficient
P	pressure
p	minimum distance between tubes
q_i	heat flux component
r	radial coordinate
TU	turbulent intensity
|U|	velocity modulus
u_i, u_j	cartesian velocity components
U_r, U_z	radial and axial velocity components
u'_i, u'_j	turbulent velocity fluctuations
x_i, x_j	cartesian coordinates
z	axial coordinate

Greek symbols

Φ	inlet gas mass flow rate
ε	turbulent dissipation rate
ω	specific turbulent dissipation rate
ρ	Density
μ	Dynamic viscosity of the gas
μ_t	turbulent viscosity
τ_{ij}	stress tensor component for i,j=1,2,3
θ	azimuthal coordinate

Subscripts

i,j	Cartesian components i,j=1,2,3
max	Maximum
r	Radial coordinate
z	Axial coordinate

1. INTRODUCTION

The steam generator (SG) of a pressurized nuclear power plant is a complex structure housing various components and around 4000 U-inverted tubes. During the plant operation a variety of phenomena may result in tube ruptures that, in case of a reactor core melting, would allow radioactive particles to be directly released to the environment. This scenario, named Steam Generator Tube Rupture (SGTR), is highly unlikely but its associated hazard turns it into a risk-dominant accident sequence.

Under normal working conditions the secondary side is flooded with water so that in the hypothetical case of an accident with fission products release, pool scrubbing would attenuate the potential radioactivity leak. However, some sequences could result in water-empty scenarios and radioactive particles would enter a "dry" secondary side carried by a high-velocity gas flow. In this case, particles could get deposited on tube surfaces within the break stage, and on the rest of structures above (i.e., support plates, tube surfaces of the subsequent stages, separators and dryers).

Herranz et al. (2007a) highlighted that aerodynamics of the gas carrying particles into the break stage of the secondary side of a "dry" steam generator is of utmost importance to fully understand the potential radioactivity retention in the break stage of a SG. They showed that particles would be mainly depleted by inertial and turbulent mechanisms. Contrarily, phoretic deposition processes were anticipated not to play any role due to the absence of thermal and steam concentration gradients in the scenario (Bakker, 2001; Güntay et al., 2002; Güntay et al., 2004).

This paper explores the aerodynamics of a gas entering the break stage through two types of breaches: guillotine and a fish-mouth, by carrying out 3D simulations with k-ω SST turbulence model and with the FLUENT code. The influence of the breach shape on the jet topology has been analyzed by comparing radial and axial velocity components along different planes. Particular emphasis has been given to the effect of the inlet mass flow rate (from 75 to 250 kg/h) on gas velocity profiles. Predictions are qualified and validated against experimental data (Velasco et al., 2007; Velasco et al., 2008)

2. COMPUTATIONAL APPROACH

The code used to investigate the 3D pattern of the gas flow was FLUENT 6.2. (Fluent, 2005). The jet motion has been modeled by using the RANS equations, which under steady state and in Cartesian form might be written as:

Continuity:
$$\frac{\partial}{\partial x_j}\rho u_j = 0 \tag{1}$$

Momentum:
$$\frac{\partial}{\partial x_j}\rho u_i u_j = -\frac{\partial}{\partial x_i}P + \frac{\partial}{\partial x_j}(\tau_{ij} - \rho\overline{u_i' u_j'}) \tag{2}$$

Energy:
$$\frac{\partial}{\partial x_j}\left[\rho u_j (h_s + \frac{u_i u_i}{2}) + u_j P + q_j - u_i \tau_{ij}\right] = 0 \tag{3}$$

Turbulence effects have been simulated by adopting the SST k-ω model, as recommended by Menter et al. (1994) in the case of flows in which adverse pressure gradients are set (typical in cylinder cross-flow configurations). This model may be understood as an evolution of the k-ω model, whose accuracy and numerical stability in the inner region of the boundary layer is supplemented with the less demanding k-ε model at the outer region of the boundary layer. A major feature of the SST k-ω model, is the consideration of the main turbulent shear stress transport, which enables to predict adverse pressure gradients. Bardina et al. (1997) extensively tested and validated two-equation eddy viscosity models and showed a better performance of the SST k-ω model in complex flows with boundary layer separation.

The transport equations (Eq. 4) of the turbulent kinetic energy (k) and its specific dissipation (ω) close the previous system, together with the Boussinesq assumption, which makes Reynolds stress tensors ($\overline{u_i' \cdot u_j'}$) proportional (μ_t) to the mean velocity gradient (Eq. 5):

$$\frac{\partial}{\partial x_i}(\rho \cdot \phi \cdot u_i) = \frac{\partial}{\partial x_j}(\Gamma_\phi \cdot \frac{\partial \phi}{\partial x_j}) + G_\phi - Y_\phi \qquad (+ D_\omega) \tag{4}$$

$$-\rho \cdot \overline{u_i' \cdot u_j'} = \mu_t \left(\frac{\partial u_i}{\partial x_j} + \frac{\partial u_j}{\partial x_i} \right) - \frac{2}{3}(\rho \cdot k + \mu_t \frac{\partial u_i}{\partial x_i}) \cdot \delta_{ij} \tag{5}$$

Where ϕ denotes the independent variable (k and/or ω) and G, Y and Γ represent generation, dissipation and effective diffusivity of the given quantity, respectively. The ω transport equation adds an additional cross diffusion term (D_ω), which arises when merging k-ω and k-ε formulation. Description of these expressions can be easily found in literature (Menter, 1994; Bardina et al., 1997; Fluent, 2005).

The whole set of equations are solved by using a segregated implicit solver with a second order discretization scheme.

The overall geometry, hypotheses and boundary conditions used in the modeling of the break stage of a tube with a guillotine type breach during a SGTR sequence are presented in the following sections. As explained before, additional simulations with a fish-mouth type breach were performed. Due to the similarities in the modeling of this scenario with the guillotine one, the following sections are focused in the guillotine breach case, whereas the fish-mouth one is presented as a parametric case later on.

2.1 Geometry and grid

Preliminary studies demonstrated that most of the jet momentum will occur in the vicinity of the breach (Herranz et al., 2005). This allowed simulating the SG break stage as if it was a square array of 11x11 tubes (0.33 x 0.33 x 1 m), supported by an upper and a lower plate (Fig.1). The bundle of tubes is bounded by vertical walls. The dimensions of the tubes and support plate are identical to those used in a stage of a SG of a nuclear power plant. The tubes are 0.019 m in diameter with a tube-to-tube spacing of 0.008 m. The broken tube is located at a central position in the bundle since the main goal of the study is to characterize the jet-tubes interaction. Such a position minimizes the effect of the bounding walls in the jet motion across the bundle. In the case of the fish mouth breach, as the jet momentum penetrates further in the bundle, the position changed to prevent from undesirable wall-jet interactions. Both breaches ($h_{guillotine}$=0.005 m, $h_{fish\text{-}mouth}$=0.04 m) are located at 0.25 m from the lower plate.

In both simulations, the flow is forced to exit through the breach and to expand across the bundle, leaving the domain through the top lid downstream the upper plate. The fluid is injected upwards at the base of the broken tube simplifying the natural motion through the bundle. Bundle configurations were identical to those of the experimental CAHT set-ups (Velasco et al., 2007, Velasco et al., 2008), whose measurements were used for validation purposes.

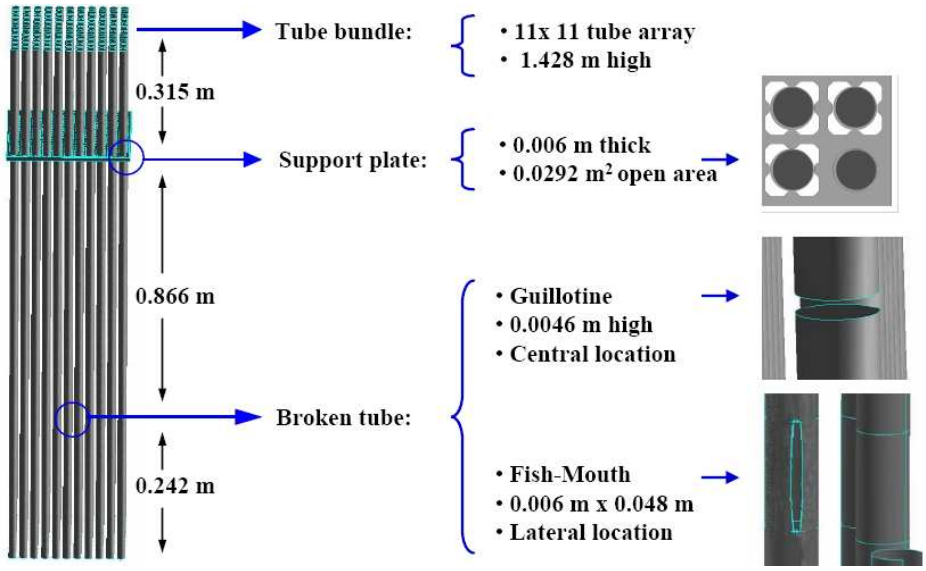

Fig. 1. Bundle configurarion.

Due to the symmetry and the breaches shape, the domain was reduced to 1/8 and 1/2 of the original one for the guillotine and fish-mouth cases, respectively. Each volume was meshed with hexahedral cells and a refined grid near the breach was set in order to capture the sharp velocity gradients of the jet shear layers (Fig. 2).

In the guillotine case, two initial grids of around 0.38 M and 1.6 M cells were defined to assess grid independence. Both of them were refined in order to describe in more detail boundary layers, which were initially described with more than 10 cells. In the fish-mouth case, the domain was discretized with a mesh of 1.2 M cells. In one of the cases, grid independence was assessed through a refined version of around 1.29 M cells, since the volume increase and the computational capabilities prevented to define a higher grid density.

Both meshes were designed according to Best Practices Guidelines (Menter et al., 2002, Mahaffy et al., 2007) so that numerical diffusion is reduced and accuracy and convergence are enhanced. As a result, a good mesh quality was achieved: In the guillotine case, 73% of the mesh had aspect ratios smaller than 50 (the remaining 27% is located in the region close to the boundary layer where higher aspect ratios are seen as acceptable); angle and size skewness were smaller than 0.1 in around 80% of the cells; and, finally, growing factors throughout the mesh were less than 1.4. In the fish-mouth case, 87% of the cells have aspect ratios smaller than 50; and angle and size skewness are smaller than 0.2 in 70% of the cells.

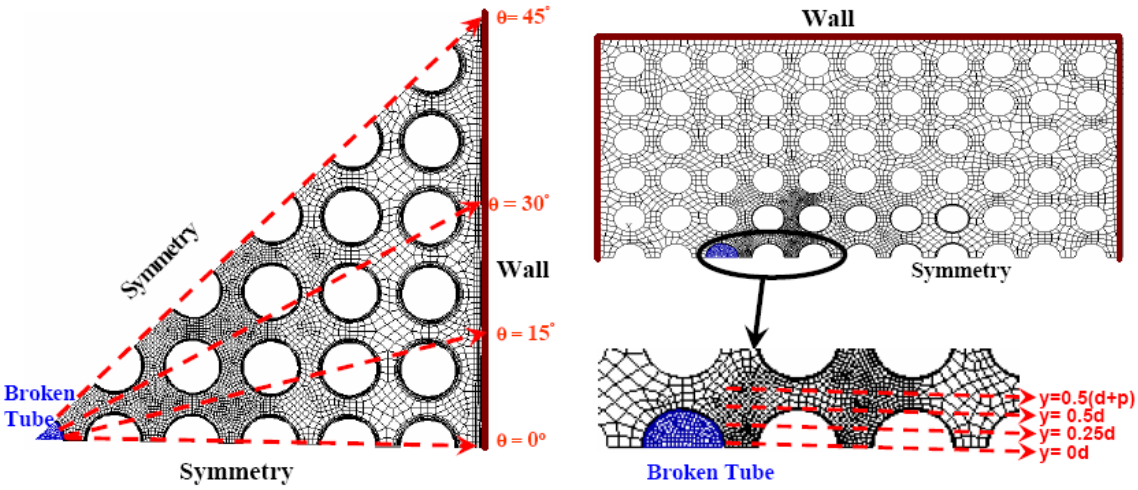

Fig. 2. Horizontal cross-section of guillotine (left) and fish-mouth (right) meshed domains.

2.2 Hypotheses and boundary conditions

Gas flow modeling and boundary conditions are similar in both guillotine and fish-mouth breach cases, reproducing as close as possible experimental conditions (Velasco et al., 2007; Velasco et al., 2008). They are summarized in the following table.

Table I. Hypotheses and boundary conditions.

Breach type		Guillotine	Fish-mouth
Compressibility		√	√
Steadiness		√	√
Turbulence model		SST k-ω	SST k-ω
Inlet	Position	Base of the broken tube	
	Φ	75, 150, 250 kg/h	75, 250 kg/h
	TU	4%	4%
Outlet	Position	Top lid of the bundle	
	p	$1.3 \cdot 10^5$ Pa	$1.2 \cdot 10^5$ Pa
	TU	7.2%	7.2%
Walls (non-slip condition)		Tubes, vertical surfaces, lower plate	
Symmetry		planes $\theta=0^o$, $\theta=45^o$	plane y = 0d
Porous media		Upper support plate	
		$\Delta P = k_1 \frac{\rho \lvert U \rvert^2}{2}$ $k_1 = 3.254$	

3. NUMERICS AND MESH-QUALITY

Two quality criteria were met by the simulations:

- Low and steady values of scaled residuals ($\leq 10^{-3}$).
- Steadiness of specific variables characterizing gas jet aerodynamics, like mean velocity, turbulent kinetic energy and specific dissipation rate.

As already said for the case of the guillotine breach, grid independence was explored through the results obtained from several meshes. It is illustrated in Table II through some aerodynamic variables particularly significant for particles deposition on tube surfaces by inertial impaction and/or eddy deposition (i.e., mean wall shear stress and velocities). As observed, these values differ in less than a 10%, and the y+ values reached ensure the good resolution of the flow within the boundary layer. Scaled residuals may be noted to meet the above criterium. In the fish-mouth breach, a refined mesh assessed this analysis for the 250 kg/h case (Table III). As observed, differences are less than a 5% and residuals reach previous low values. However, y+ values exceed the recommended maximum 5 (Fluent, 2005). It must be noticed that these values are an average over the whole domain and at those surfaces of highest turbulence in the region close to the breach, these values are reduced to around 1.5.

Table II. Numerical properties and results of guillotine simulations.

Φ	75 kg/h		150 kg/h		250 kg/h	
Grid	Coarse	Fine	Coarse	Fine	Coarse	Fine
Number of cells	379760	1582905	373334	1582905	431546	1582905
Scaled Residuals	10^{-4}	10^{-3}	10^{-3}	10^{-3}	10^{-4}	10^{-4}
Discretization	2nd order	2nd order	2nd order	2nd order	2nd order	2nd order
Mean y+	1.14	0.47	1.85	1.09	2.63	1.35
Mean wall shear stress (Pa)	0.05	0.042	0.17	0.164	0.36	0.38
$\|U\|_{max}$ (m/s)	89	90	160	167	248	250
$\|U\|_{mean,\ breach}$ (m/s)	62.41	64.34	116	120.2	170.77	175
$\|U\|_{mean,\ outlet}$ (m/s)	0.186	0.208	0.37	0.41	0.63	0.69

Table III. Numerical properties and results of fish-mouth simulations.

Φ	75 kg/h	250 kg/h	
Number of cells	1200195	1200195	1288633
Scaled Residuals	10^{-5}	10^{-5}	10^{-5}
Discretization	1st and 2nd order	1st and 2nd order	1st and 2nd order
Mean y+	11	24	23
Mean wall shear stress (Pa)	0.07	0.43	0.44
$\|U\|_{max}$ (m/s)	163	379	369
$\|U\|_{mean,\ breach}$ (m/s)	114	248.6	246
$\|U\|_{mean,\ outlet}$ (m/s)	0.3	0.68	0.69

From now on, the layout of the results will be presented in cylindrical coordinates (r, θ, z) whose axial origin is set at the lower part of the breach and the radial one, starts just at the surface of the broken tube.

Fig. 3 displays an example of the velocity profiles along two vertical lines placed at different (r, θ) locations for the guillotine case (Φ = 250 kg/h). The maximum corresponds to the velocity of the jet emerging from the break into the secondary side. At this location as well as at both sides of the maximum, both meshes provide the same flow behavior. In absolute values, velocity magnitudes agree, deviations being less than 15% at the jet core.

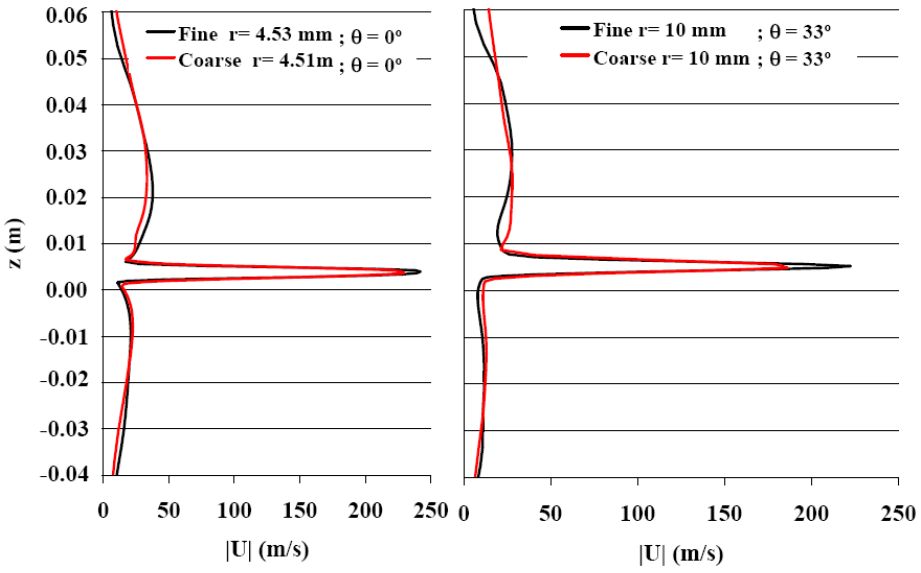

Fig. 3. Velocity profiles along two vertical lines (left: r= 4.5 mm, θ=0°; right: r=10 mm, θ=33°).

4. Validation

Validation of the simulations was carried out against a data base built-up for this purpose (Velasco et al., 2007, Velasco et al., 2008). A mock-up facility consisting of a tube bundle of 11x11 rows was used to simulate the break stage of the SG. The bundle was bounded by a vertical methacrylate structure that permitted the investigation of the jet aerodynamics with optimal optical access. A standard 1660x1200 pixels PIV cross-correlation CCD camera, a pulsed Nd:Yag laser and two different lenses (28 and 300mm F2.8) were used to record the images. Additionally, a Pitot tube was used to characterize specific regions of the fluid domain. Uncertainties in PIV and Pitot tube measurements of the mean velocity field have been estimated to be less than 35% and 10%, respectively, within a 95% of confidence level. The inlet tube mass flow rate was varied in the experiments from 75 to 250 kg/h. TiO_2 was used as seeding material.

Fig. 4 compares predictions obtained in the space between the broken tube and the first neighbor and the equivalent PIV measurements of velocity fields acquired in the experimental campaign for both breaches. Blank contours in the guillotine simulations mean that velocities in those regions were higher than the range plotted (i.e., up to 52 m/s). Overall, the experimental description and the theoretical one were consistent:

- Guillotine breach results show that once impacting the neighbor tube, the gas exiting the breach in form of a jet splits in upwards, downwards and sidewards streams (just the two former can be observed in the plot). The jet causes a noticeable entrainment of the fluid around, both at the upper and at the lower region. Nonetheless, again consistently with data, simulations anticipate a more substantial suction above than below the jet. This is due to the parabolic trajectory of the jet that fosters a recirculation in the concave region. This trajectory results from the combination of three factors: the initial vertical component of the jet; the presence of tubes, which fosters gas motion along tube surfaces (Coanda effect, i. e. adhesion of a fluid to a curved surface, Schuh et al.; 1964); and the gas drift due to the location of gas exit at the top of the facility.
- The fish-mouth case (Φ = 75 kg/h) results show the jet exiting the breach. The normalized PIV measurements and simulation were qualitatively consistent, namely both trends agree on flow orientation and velocity profile shape: they display a quasi top-hat velocity profile and the vectors orientation is similar except for the lower region of the breach, where PIV data slightly increases with respect to mid and upper regions.

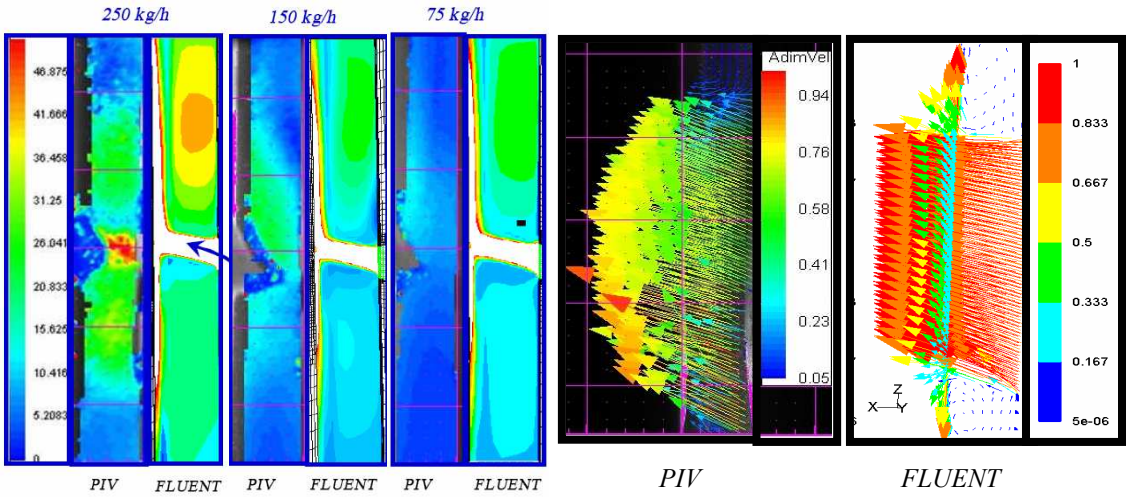

Fig. 4. PIV, FLUENT guillotine velocity contours (left), fish-mouth velocity vectors (right).

Fig. 5 allows a quantitative comparison between predictions and data along one vertical line located at θ=0° and at 1/3 of tubes spacing. As observed, the figure includes complementary

Pitot tube data at 1/3 of the tube spacing obtained in a free jet configuration. As discussed by Velasco et al. (2008), they provide more reliable velocities in the region of jet core near the breach as PIV measurements in this location suffer from some experimental drawbacks. This comparison is considered meaningful since at such a short distance from the breach, no major effects on velocity magnitude due to the presence of tubes are expected.

In both cases, simulations captured the experimental profile and its accuracy can be considered reasonable:

- Guillotine: Major deviations found in the core region are around 8% with respect to the Pitot tube readings. As observed, there are slight discrepancies between simulations and PIV measurements at both sides of the jet core. However, predictions are well within the experimental uncertainty band.
- Fish-mouth: Simulation estimates and PIV data discrape around a 50% whereas the comparison to Pitot readings shows an outstanding qualitative and quantitative agreement, which support simulations consistency.

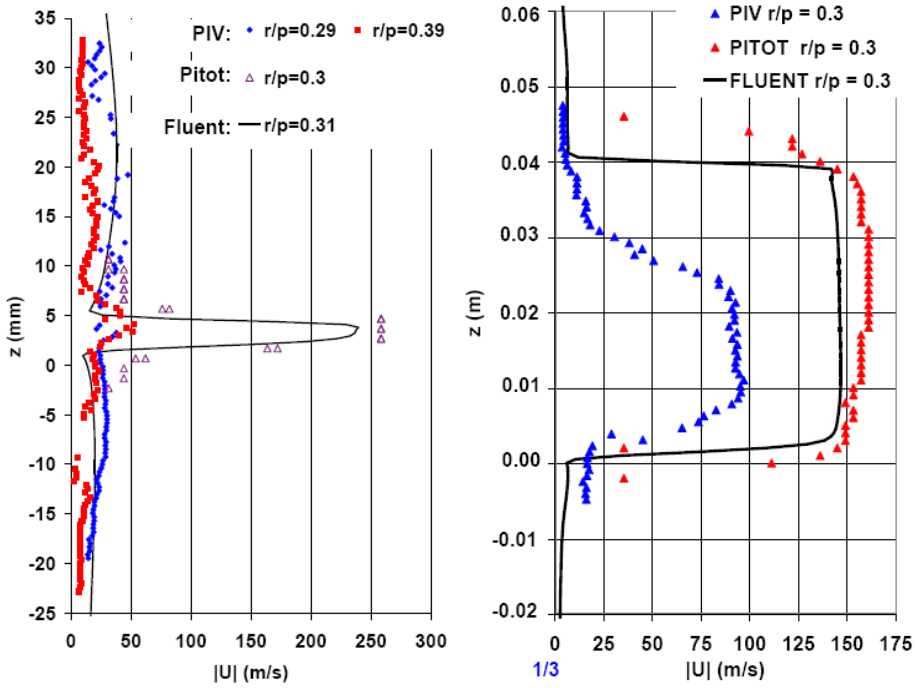

Fig. 5. Vertical velocity profiles at θ=0° and r/p =1/3 for guillotine (left, 250 kg/h) and fish-mouth (right, 75 kg/h).

5. Results

The analyses of the simulations were essentially focused on the characterization of jets across the bundle for both breach configurations.Their differences and similarities as well as the influence of the inlet mass flow rate are shown in terms of the radial and axial velocity components at different planes.

5.1 Jet evolution

Jets evolution across the bundle can be observed in Fig. 6, which shows the velocity fields at different heights (250 kg/h). It is noteworthy that in quantitative terms, colors have a different meaning in each plot, since the scales are different.

Both jets leave the breach drawing a quasi-parabolic shape with a high initial radial displacement, whose trayectory is affected radially and axially by the presence of the tubes (Fig. 5, Fig. 6). In the guillotine case, the jet distributes evenly over the entire azimuthal direction. As the jet impinges on tubes two major effects are observed. In the radial direction, impingement on the tubes makes the jet flow along diagonal directions since resistance is

minimum (fewer obstacles). In the axial direction, once the jet impinges on the tube surface, a fraction of the jet is driven upwards around the tube, as if it was attached. This behavior may be attributed to the so called "Coanda effect" (Schuh et al., 1964; Schlichting et al., 2000), and it becomes more noticeable as the radial momentum becomes small. The net result is an enhancement of the axial orientation of the jet. As noted, in the fish-mouth case the circumferential symmetry vanishes and the jet expands azimuthally in a pseudo-triangular way. It hits almost entirely the facing tube row moving essentially parallel to it. Once the jet is intercepted by each tube, a fraction is diverted upward until eventually escapes through the top lid of the bundle.

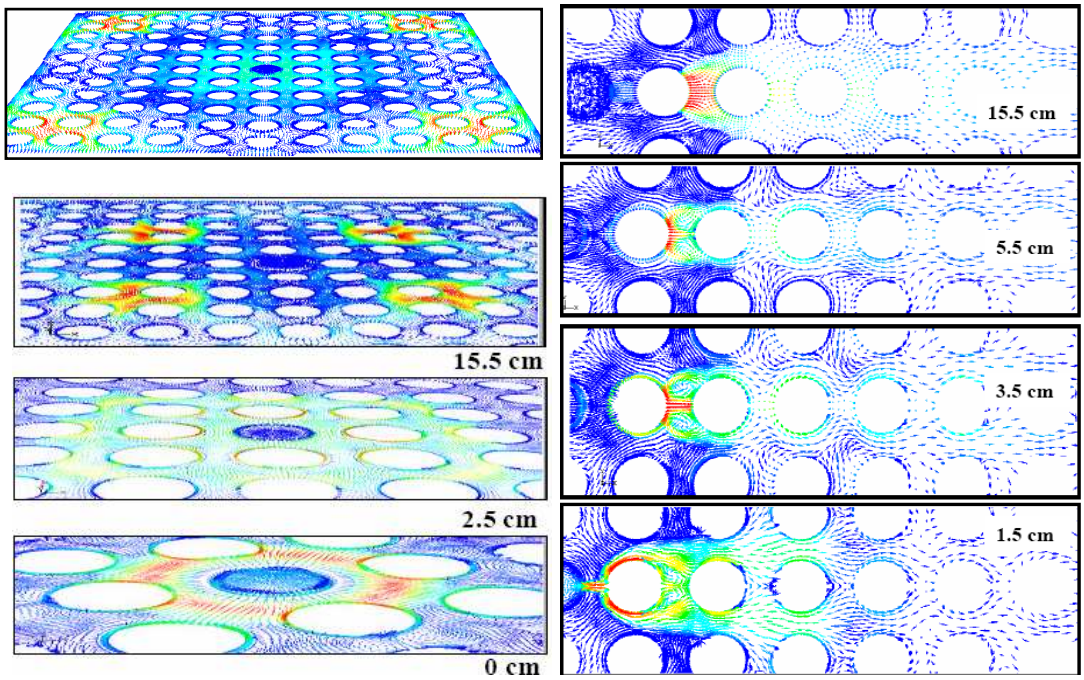

Fig. 6. Velocity vectors at different heights (250 kg/h): guillotine (left), fish-mouth (right).

Radial and axial velocity components were analyzed along different planes trying to follow each jet trajectory: four azimuthal directions (0º, 15º, 30º and 45º) for the guillotine breach and four parallel planes (y=0·d, 0.25·d, 0.5·d and 0.5·(d+p)) for the fish-mouth one (Fig. 2).

Fig. 7 shows the normalized maximum radial velocity as a function of the distance from the breach (250 kg/h). The latter is expressed in a dimensionless way by defining a unit length as the distance from the breach to the first tube in each of the directions analyzed (black vertical lines in the plot representing a tube location). Note that velocity normalizations were performed independently for each case.

In the guillotine case, radial velocity reaches a maximum at around 1/3 of the first spacing (expansion effect due to the pressure drop at the breach) and decreases differently depending on direction. Along 0º and 45º, where the jet impinges the first neighbor tube surface in a nearly cross flow configuration, velocities sharply decrease at the vicinity of tube surface. At directions 15º and 30º, the jet does not approach the tubes normally but tangentially, which makes their radial velocity evolve in a rather continuous way. On 0º and 45º planes, it may be noted that radial velocity reaches a secondary maximum in between first and second neighbor tubes. In fact, those maxima might be observed on any plane touching the tube surface. However, the collapse in a non-dimensional axis (which requires to shrink tube width at each azimuthal plane into a single point at the x axis), prevents that observation on planes out of the perpendicular direction to the tubes. Those maxima are located adjacent to the wake region caused by the boundary layer detachment, so that they appear at longer distances on those planes oriented perpendicularly to the tube axis (i.e., 0º and 45º). Regardless direction, from the second tube on, normalized radial velocities nearly vanish to less than 5% of the inlet velocity.

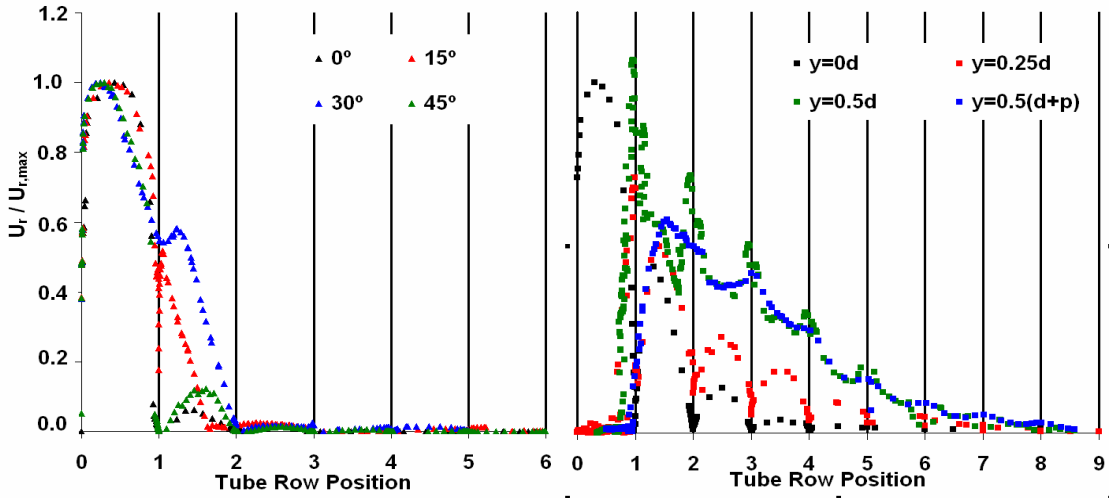

Fig. 7. Normalized maximum radial velocity (250 kg/h): guillotine (left), fish-mouth (right).

In the fish-mouth case, the jet also expands when exiting the breach, reaching a maximum radial velocity at 1/3 of the spacing between the breach and the first neighbor (y=0·d, Fig. 7). As observed in this spacing, planes other than y=0·d do not notice initially the jet stream due to the jet slot-like shape that constrains the jet width. They show the distances required for the initially quiescent gas to get sucked by the jet, reaching their maxima velocities close to the first tube. From then on, radial velocity decreases differently depending on the plane. Along y=0·d and y= 0.25·d, the jet also impinges the tubes in a nearly cross-flow configuration displaying similar bumps to what has been shown in guillotine profiles (planes 0º and 45º). However, the latter presents lower velocities because of its larger exchange surface with the surroundings, which enhances momentum loss. Therefore, jet radial penetration is higher in the fish-mouth configuration than in the guillotine one.

The highest maximum radial velocities are reached along planes y=0.5·d and y=0.5·(d+p) as the jet flows almost freely without obstacles. Their decreasing rate is also milder than those of the previous planes intercepting the tubes. Furthermore, along plane y=0.5·d the gas presents peaks of maxima velocities where it touches tangentially the tubes. They result from the acceleration of the gas flowing over the tube surface in the favorable pressure gradient direction. This is also observed in the guillotine profile, the maximum at 1/3 of the second spacing of plane 30º shows the acceleration of the gas flowing close to the rear of the facing diagonal neighbor tube.

The normalized maximum axial velocities are shown in Fig. 8, where axial position (z) was normalized with the breach height (h). As observed, for both breach configurations this velocity decreases when increasing the axial distance from the breach. The maximum values are attained in the plane facing the breach (along 0º and y=0·d directions), as the radial momentum of impacting jet (transformed into the axial) is higher at that location.

Regardless azimuthal direction in guillotine profiles, axial velocities decrease to 10% of the maximum at the axial distance z/h of around 20. From then on, velocity keeps on diminishing but with a milder slope.

Regarding fish-mouth profiles, velocities of planes intercepting the tubes evolve in a similar way, whereas the other ones behave differently. Those differences found with planes y= 0.5·d and y=0.5·(d+p) at z/h ratios lower than 5 indicate the evolution of the quiescent surrounding gas when influenced by the jet. From this value on, axial velocities converge reaching a 10% of the maximum at z/h around 14.

The comparison of both configurations shows a faster decay and lower velocities for the fish-mouth breach than the guillotine one until z/h around 5, where both velocities reach around a 30% of their maximum. From that value on, both velocities decrease similarly. It must be noticed that fish-mouth breach height is 10 times larger than the guillotine one. Therefore, in

absolute values a larger region of the bundle would undergo a higher influence of the jet in the case of a fish-mouth breach than in the case of a guillotine one.

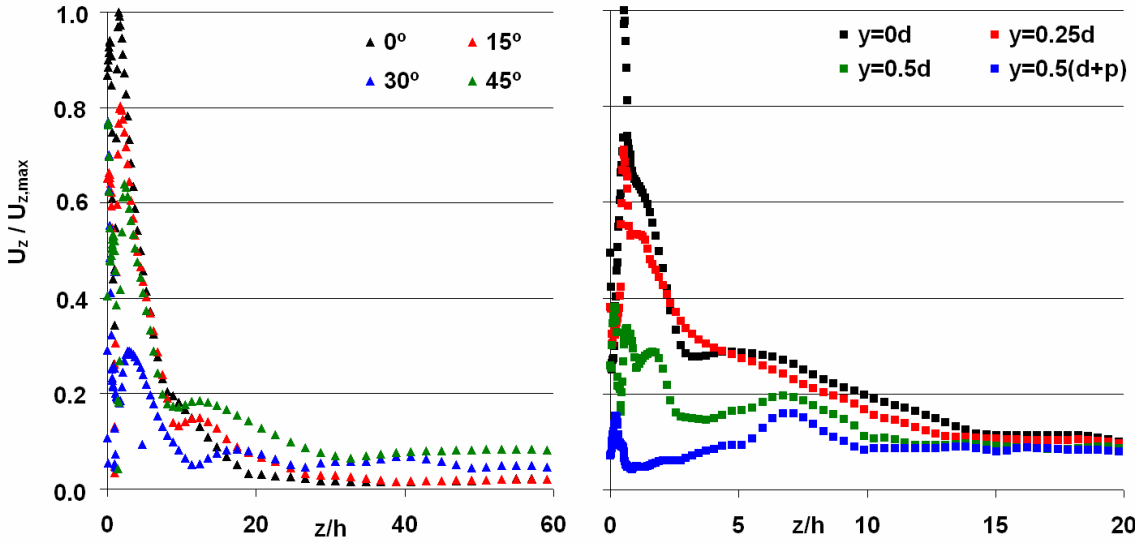

Fig. 8. Normalized maximum axial velocity (250 kg/h): guillotine (left), fish-mouth (right).

5.2 Effect of the mass flow rate

The effect of the initial mass flow rate is presented in terms of the maximum radial and axial velocity profiles for the guillotine breach configuration (Fig. 9). As observed from the figure, the inlet mass flow rate does not yield any difference in the radial or axial jet behavior. In other words, the decreasing trends of the radial and axial velocities as the jet penetrates across the tube bundle have a generic nature. Of course, when the natural distances are considered, velocities hold noticeable values at deeper or higher locations at high mass flow rates. Therefore, the highest mass flow rate the deeper penetration.

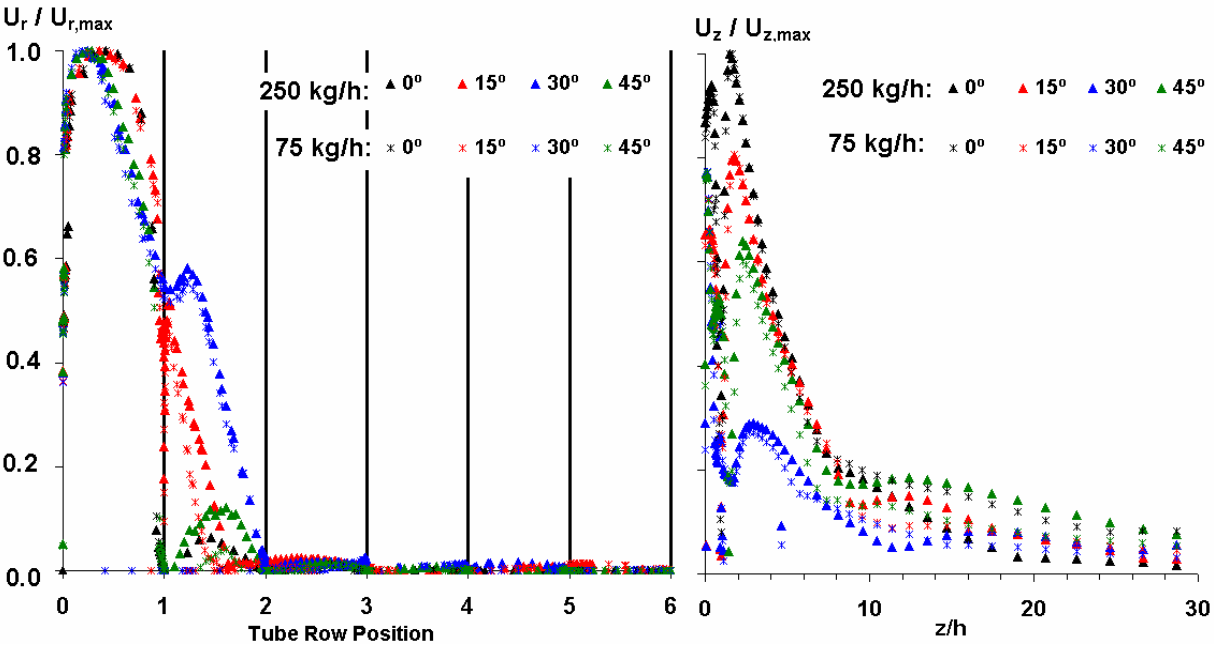

Fig. 9. Normalized maximum radial (left) and axial (right) velocity profiles (75, 250 kg/h).

6. Conclusions

This work summarizes the 3D CFD modeling of the aerodynamics of a jet emerging from a guillotine and a fish-mouth breach into the break stage of a dry steam generator during SGTR sequence. The scenario was modeled using the SST k-ω turbulent model. Best practices guidelines were followed and results were proven to be grid independent and agreed with the experimental database. The CFD modeling of the jet has provided valuable insights into the jet behavior across the bundle.

The results showed that the jet behaves in a different way depending on the breach type. In case of the guillotine breach, it evolves within the tube bundle following a generic quasi-parabolic pattern with azimuthal symmetry. Initially, it is dominated by the radial velocity component, followed by a progression mainly in the diagonal direction with a dominant axial velocity component. In case of a "fish-mouth jet", the azimuthal domain of the jet is limited to less than $\pm 25^{o}$ and the jet distribution in the radial and axial direction occur at the same time. So to say, during the jet penetration in the bundle, a fraction of mass flow rate is diverted upwards.

Regarding velocity magnitudes, jets from fish-mouth breaches reach further radial and axial distances than those from guillotine ones for the same initial mass flow rate. The faster velocity decrease of guillotine velocities might be a consequence of its larger surface exchange area when compared to the fish-mouth one. Regarding inlet mass flow rate, it was seen that for the guillotine breach configurations it influences the jet in absolute terms, namely deeper penetration are reached at higher mass flow rates. However, in relative terms the normalized maximum radial and axial velocities were shown to be self-similar.

In the scenario analysed the principal aerosol deposition processes foreseen are inertial impaction and turbulent deposition. Both mechanisms are intrinsically linked to the aerodynamics of the gas carrying the particles. The deep understanding of the in-bundle gas motion gained through these 3D analyses will make it possible to encapsulate the gas jet description in 1D theoretically based correlations. By doing so applicability of these studies to nuclear safety will be straightforward since 1D correlations are fully compatible with current architecture of nuclear safety codes.

Acknowledgements

The authors wish to thank the Spanish Nuclear Safety Council for the financial support of this research and other partners of the international ARTIST project, under which this research has been conducted, for their helpful technical input.

REFERENCES

Bakker P., Slootman M., Dienstbier J., Güntay S., Herranz L., Jokiniemi J., Routamo T., 2001. "Accident Management Aspects of EU-SGTR Project", NEA/CSNI/R(2001)20 Proc of the Workshop on Implementation of Severe Accident Management Measures., Villigen, Switzerland.

Bardina J.E., Huang P.G., Coakley T.J., 1997. "Turbulence Modeling Validation, Testing and Development." NASA Technical Memorandum 110446.

FLUENT, 2005. FLUENT 6.2 Users Guide. Lebanon, USA.

Güntay S, Dehbi A, Suckow D, Birchley J (2002) "ARTIST: an international project investigating aerosol retention in a ruptured steam generator". Int congress on advanced nuclear power plants ICAPP'02, June 9-13, Hollywood, Florida.

Güntay S., Suckow D., Dehbi A., Kapulla R., 2004. "ARTIST: introduction and first results". Nucl Eng Des Vol.231, pp.109-120.

Herranz L.E., Del Prá C.L., Dehbi A., 2007(a). "Major Challenges to modeling aerosol retention near a tube breach during steam generator tube rupture sequences." Nucl Tech Vol.158, pp.83-93.

Herranz L.E., López del Prá C., Sánchez Velasco F.J., 2007(b). "Preliminary steps toward assessing aerosol retention in the break stage of a dry steam generator during severe accident SGTR sequences", Nucl Eng Des,doi:10.1016/j.nucengdes.2007.10.007

Herranz L., Del Prá C.L., Velasco F.J.S., Muñoz-Cobo J.L., Escrivá A, 2005. "Insights into aerosol depletion from a high velocity flow across a tube bank: a key scenario for nuclear safety." Proc of 6th World conf on experimental heat transfer, fluid mechanics and thermodynamics. April 17-21, Miyagi, Japan.

Leaver D.E., Li J., Sher R., 1998. "New Design Applications of Natural Aerosol Deposition in Nuclear Plant Accident Analyses", NEA/CSNI/R(98)4.

Mahaffy J., Chung B., Dubois F., Ducros F., Graffard E., Heitsch M., Henriksson M., Komen E., Moretti F., Morii T., Muhlbauer P., Rohde U., Scheuerer M., Smith B. L., Song C., Watanabe T., Zigh G., 2007. "Best Practice Guidelines for the use of CFD in Nuclear Reactor Safety Applications". NEA/CSNI/R(2007)5.

Menter F., Hemstrom B., Henriksson M., Karlsson R., Latrobe A., Martin A., Muhlbauer P., Mscheuerer, Smith B., Takacs T., Willemsen S., 2002. "CFD Best Practice Guidelines for CFD Code Validation for Reactor-Safety Applications". ECORA, Contract FICKS-CT-2001-00154.

Menter F.R., 1994. "Two-Equation Eddy-Viscosity Turbulence Models for Engineering Applications." AIAA Journal, Vol 32, pp.1598-1605.

Meyer K.E., 1994. "Experimental and numerical investigation of turbulent flow and heat transfer in staggered tube bundles". PhD. Thesis, Technical University of Denmark.

Schlichting H., Gersten K., 2000. "Boundary Layer Theory". Chap. 12.2.3. Ed Springer.

Schuh H., Persson B., 1964. "Heat transfer on circular cylinders exposed to free-jet flow." Int J Heat Mass Transfer Vol.7, pp.1257-1271.

Velasco F.J.S., López del Prá C., Herranz L.E., 2007. "Jet Expansion from a Fish-Mouth Tube Breach in a Shell and Tube Heat Exchanger". 7th Int. Symp. On Particle Image Velocimetry, 11-14th September, Rome (Italy).

Velasco F.J.S., López del Prá C., Herranz L.E., 2008. "Expansion of a radial jet from a guillotine tube breach in a shell-and-tube heat exchange"r. Exp. Therm. Fluid Sci., 32,947-961.